

Very blue-shifted broad H α in a low redshift Type-1.9 AGN: a disk emitter or a recoiling black hole scenario

Xue-Guang Zhang¹★

¹ *Guangxi Key Laboratory for Relativistic Astrophysics, School of Physical Science and Technology, Guangxi University, 530004, Nanning, P. R. China*

1 February 2024

ABSTRACT

In this manuscript, very blue-shifted broad H α with shifted velocity ~ 2200 km/s is reported in the low redshift Type-1.9 AGN SDSS J1052+1036. Blue-shifted broad emission lines may arise due to the presence of a rotating gas disk around central black hole (BH), but may also be a signature of rare phenomena such as gravitational wave recoil of a supermassive BH (rSMBH) or the presence of a binary BH (BBH) system. Here, due to larger shifted velocity of stronger and wider blue-shifted broad H α , the BBH system is disfavoured. Meanwhile, if this object contained a rSMBH, intrinsic obscuration with $E(B-V) \leq 0.6$ should lead to a detectable broad H β , indicating the rSMBH scenario not preferred. We find that the blue-shifted broad H α can be well explained by emission from an AGN disk, indicating that SDSS J1052+1036 is likely a disk-emitting AGN. In order to determine which scenario, a rSMBH or a disk emitter, is more preferred, a re-observed spectrum in 2025 can provide robust clues, with a disk emitter probably leading to clear variations of peak positions, peak separations and/or peak intensity ratios in broad H α , but with a rSMBH scenario probably leading to no variations of peak separations in broad H α .

Key words: galaxies:active - galaxies:nuclei - quasars:emission lines - quasars: individual (SDSS J1052+1036)

1 INTRODUCTION

Shifted broad emission lines relative to stellar absorption features (or narrow emission lines) may be indicators of a gravitational wave recoiling supermassive black hole (rSMBH) in called off-nucleus active galactic nuclei (AGN), due to gravitational wave carried off linear momentum leading central BH being kicked away from central region of AGN, as discussed in [Bekenstein \(1973\)](#); [Madau & Quataert \(2004\)](#); [Merritt et al. \(2006\)](#); [Volonteri \(2007\)](#); [Blecha & Loeb \(2008\)](#); [Komossa & Merritt \(2008a\)](#); [Blecha et al. \(2016\)](#). Broad emission lines from broad emission line regions (BLRs) bound to a rSMBH with a large kick velocity can lead to blue-shifted broad emission lines relative to narrow emission lines of AGN, due to no effects of a rSMBH on NLRs (narrow emission line regions). Until now, there are a few individual AGN and samples of AGN reported with blue-shifted broad emission lines, and expected rSMBH scenarios have been discussed in the literature.

[Komossa et al. \(2008\)](#) have reported SDSS J0927+2943 ($z \sim 0.713$) with blue-shifted velocities 2650 km/s in broad emission lines, to support a rSMBH scenario. However, [Bogdanovic et al. \(2009\)](#) have discussed a binary BH (BBH) system with mass ratio 0.1 also leading to the shifted features in SDSS J0927+2943. [Shields et al. \(2009\)](#) have reported blue-shifted velocity 3500 km/s in broad H β in SDSS J1050, however, BLRs lying into central accretion disk (=disk emitter) would be preferred to explain the blue-shifted broad H β , rather than the rSMBH scenario. [Steinhardt et al. \(2012\)](#) have reported very blue-shifted broad emission lines in SDSS J0956+5128, however, either an extreme disk emitter or a rSMBH is not the preferred scenario to explain all of the observed features, especially

the different profiles between broad Balmer lines and broad Mg II line. [Kim et al. \(2017\)](#) have discussed the rSMBH candidate of CXO J1015+6259 ($z \sim 0.35$) with blue-shifted velocity 175 km/s in broad emission lines. [Kalfountzou et al. \(2017\)](#) have shown a rSMBH is one proposed scenario to explain the three strong emission-line nuclei with velocity offset 250 km/s in SDSS J1056+5516 ($z \sim 0.256$), as well as a triple BH accreting system. [Kim et al. \(2018\)](#) have applied an oscillating rSMBH scenario to explain the broad emission line variability properties in Mrk1018. [Chiaberge et al. \(2017, 2018\)](#); [Morishita et al. \(2022\)](#) have shown that the quasar 3C186 ($z \sim 1.07$) have blue-shifted velocity 2140 km/s in broad emission lines, consistent with expected results by a rSMBH.

Meanwhile, there are samples of AGN with blue-shifted broad emission lines. [Eracleous et al. \(2012\)](#) and followed in [Runnoe et al. \(2015, 2017\)](#) have reported a sample of tens of low redshift ($z < 0.7$) SDSS quasars with blue-shifted velocities larger than 1000 km/s in broad H β , and discussed that BBH systems should be preferred in a fraction of the candidates, after carefully checked changes of peak velocities through multi-epoch spectra. [Lena et al. \(2014\)](#) have shown 10 rSMBH candidates in nearby galaxies with small displacements between central activity region and center of galaxy. [Kim et al. \(2016\)](#) have reported a sample of candidates with mean blue-shifted velocity about 150 km/s for rSMBHs in SDSS quasars with redshift less than 0.25. [Ward et al. \(2021\)](#) have shown nine AGN that may be spatially offset from their host galaxies and are considered as candidates for rSMBHs.

Based on the reported candidates of AGN with blue-shifted broad emission lines, besides the rSMBH scenarios, either the BBH or disk emitter hypotheses can be applied. Moreover, as discussed in [Komossa & Merritt \(2008b\)](#); [Shen et al. \(2019\)](#), candidates of rSMBHs with large recoiling velocities at low redshift are ex-

★ Corresponding author Email: xgzhang@gxu.edu.cn

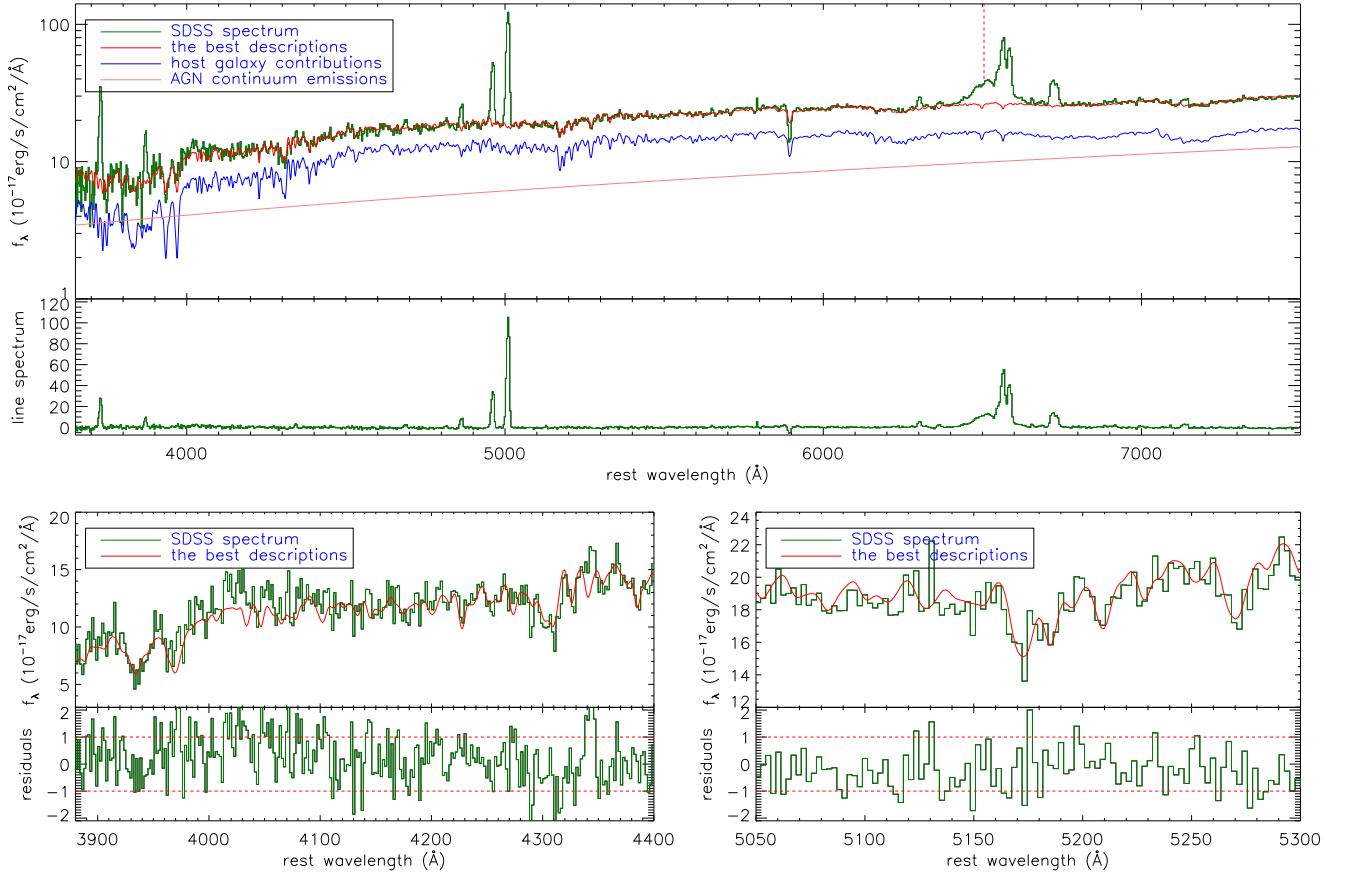


Figure 1. Top region of the top panel shows the SSP method determined the best descriptions (solid red line) to the SDSS spectrum (solid dark green line) with emission lines being masked out. Solid blue line and solid pink line show the determined host galaxy contributions and the power law AGN continuum emissions, vertical dashed red line marks the blue-shifted broad H α . Bottom region of the top panel shows the pure line spectrum by the SDSS spectrum minus the sum of the host galaxy contributions and the power law AGN continuum emissions. Top regions and bottom regions of the bottom panels show the best fitting results (solid red line) and the corresponding residuals (the line spectrum minus the best fitting results and then divided by uncertainties of the SDSS spectrum) to the absorption features (solid dark green line) around the Ca II H+K (bottom left panel) and around the Mg I (bottom right panel). In the bottom region of each bottom panel, horizontal red dashed lines show residuals= ± 1 , respectively.

tremely rare. Here, a candidate at redshift 0.088 is reported with blue-shifted velocity ~ 2200 km/s in broad H α in a Type-1.9 AGN SDSS J105232.97+103620.08 (=SDSS J1052+1036), with different scenarios discussed. This manuscript is organized as follows. Section 2 presents the spectroscopic results of the Type-1.9 AGN SDSS J1052+1036. Section 3 gives main discussions. Section 4 gives our final conclusions. And the cosmological parameters have been adopted as $H_0 = 70 \text{ km} \cdot \text{s}^{-1} \text{ Mpc}^{-1}$, $\Omega_\Lambda = 0.7$ and $\Omega_m = 0.3$.

2 MAIN RESULTS

SDSS J1052+1036 is selected as the subject of this manuscript, due to its very blue-shifted broad H α , while studying properties of double-peaked narrow emission lines in low redshift ($z < 0.35$) SDSS quasars including some objects reported in the sample of Ge et al. (2012). SDSS J1052+1036 has its SDSS spectrum (plate-mjd-fiberid=1602-53117-0243) with signal-to-noise about 18 shown in top left panel of Fig. 1 with apparently shifted broad H α marked by vertical dashed red line.

In order to measure the emission lines as well as to measure the stel-

lar velocity dispersion, the commonly accepted SSP (Simple Stellar Population) method is applied to determine host galaxy contributions in SDSS J1052+1036. More detailed descriptions on the SSP method can be found in Bruzual & Charlot (2003); Kauffmann et al. (2003); Cid Fernandes et al. (2005); Cappellari (2017). The SSP method has also been applied in our previous papers Zhang (2021a,b,d, 2022a,b). Here, we briefly describe the SSP method. The 39 simple stellar population templates from Bruzual & Charlot (2003); Kauffmann et al. (2003) are applied to describe stellar lights, combined with a power law function to describe the AGN continuum. When the SSP method is applied, narrow emission lines are masked out by full width at zero intensity about 450 km/s, and the spectrum with wavelength range from 6450 Å to 6750 Å are also masked out due to the strongly broad H α . Then, through the Levenberg-Marquardt least-squares minimization technique (the MPFIT package), SDSS spectrum in rest frame with emission lines being masked out can be well described. The best descriptions and the corresponding line spectrum (SDSS spectrum minus the best descriptions) are shown in the top panel of Fig. 1 with $\chi^2/dof \sim 1.26$ (the summed squared residuals divided by degree of freedom). Considering the totally obscured broad H β , the determined red power law continuum emissions was

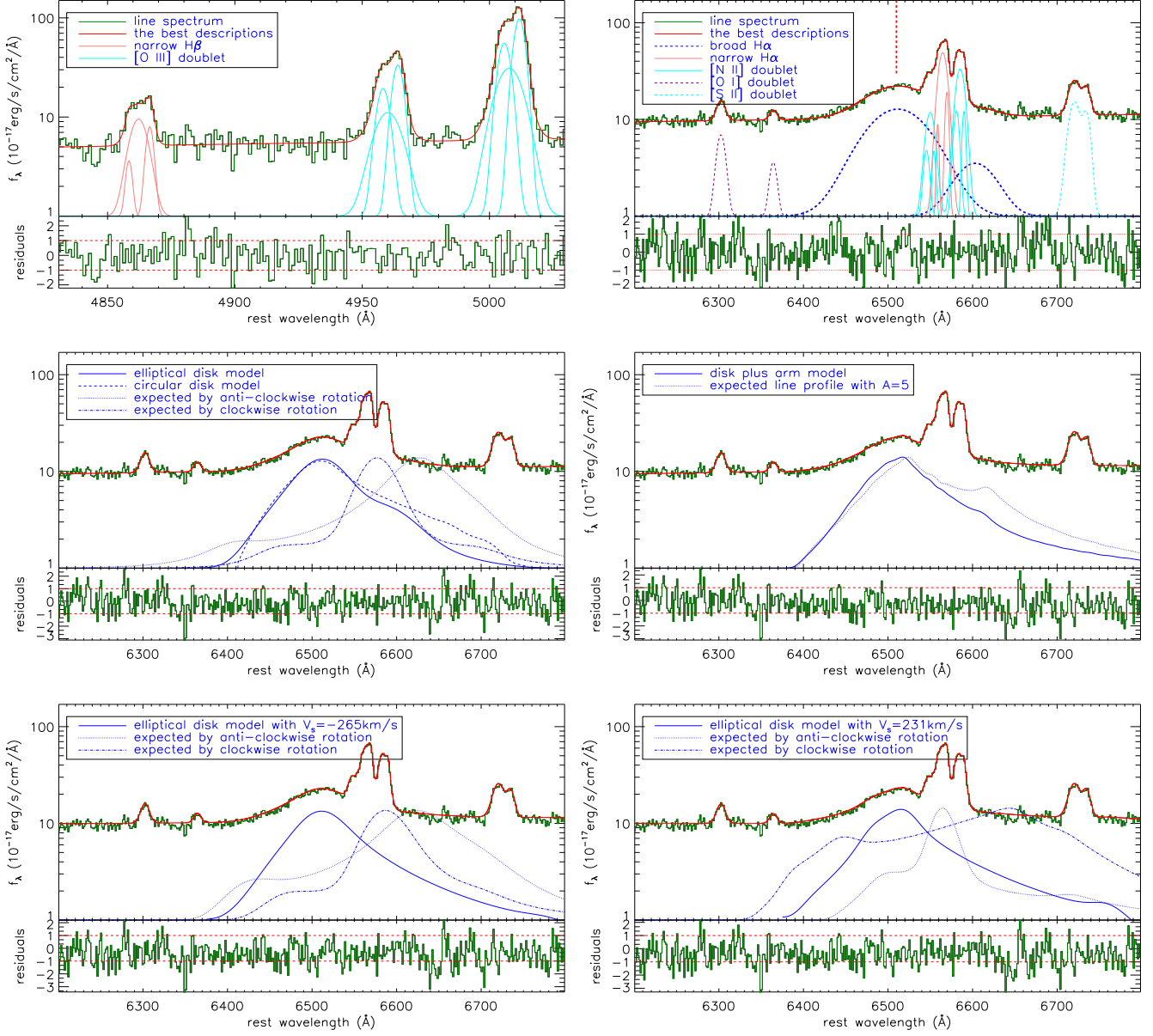


Figure 2. Top left panel shows the best fitting results (solid red line) (top region) and the corresponding residuals (bottom region) to the emission lines around the H β (solid dark green line) by multiple Gaussian functions. In top region of the top left panel, solid pink lines show the three Gaussian components in the narrow H β , solid cyan lines show the six Gaussian components in the [O III] doublet. Top right panel shows the best fitting results (solid red line) (top region) and the corresponding residuals (bottom region) to the emission lines around the H α (solid dark green line) by multiple Gaussian functions. In top region of the top right panel, solid pink lines show the three Gaussian components in the narrow H α , solid cyan lines shows the six Gaussian components in the [N II] doublet, dashed purple lines and dashed cyan lines show the Gaussian components in the [O I] and [S II] doublets, thick dashed blue lines show the two broad Gaussian components in the broad H α . Middle left panel shows the best fitting results (solid red line) (top region) and the corresponding residuals (bottom region) to the emission lines around the H α , with the elliptical accretion disk model applied to describe the broad H α . In top region of the middle left panel, solid blue line shows the determined broad H α by the elliptical accretion disk model, dotted blue line and dot-dashed blue line represent the expected line profiles of the broad H α in Jul. 2025 with considering the standard elliptical accretion disk model applied with anti-clockwise rotation and clockwise precessions respectively, dashed blue line shows the determined broad H α by a circular accretion disk model with $e = 0$. Due to totally similar descriptions to the narrow emission lines, the Gaussian components are only shown in the top right panel for the narrow emission lines around the H α . Middle right panel shows the best fitting results (solid red line) (top region) and the corresponding residuals (bottom region) to the emission lines around the H α , with the circular accretion disk plus spiral arm model applied to describe the broad H α . In top region of the middle right panel, solid blue line shows the model determined broad H α , dotted blue line shows the expected line profile of the broad H α determined by the circular disk plus spiral arm model with different A . Bottom panels show the best fitting results (solid red line) (top regions) and the corresponding residuals (bottom regions) to the emission lines around H α , with the elliptical accretion disk model with $V_s = -265$ km/s (bottom left panel) and with $V_s = 231$ km/s (bottom right panel) applied to describe the broad H α . In top regions of the bottom panels, dotted blue line and dot-dashed blue line represent the expected line profiles of broad H α in Jul. 2025 with considering the standard elliptical accretion disk model with $V_s = -265$ km/s (bottom left panel) and with $V_s = 231$ km/s (bottom right panel) applied with anti-clockwise rotation and clockwise precessions respectively.

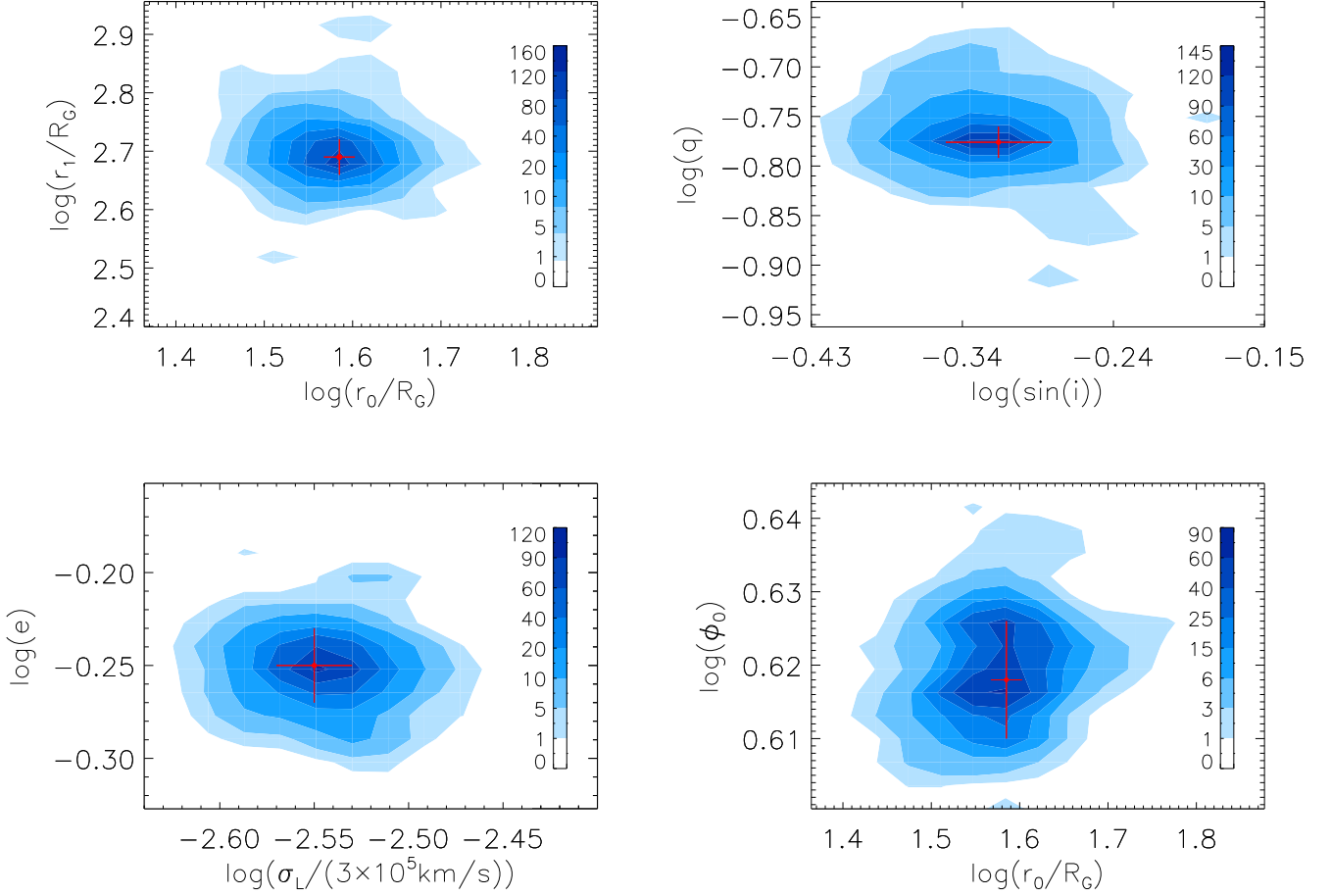


Figure 3. MCMC technique determined two-dimensional posterior distributions in contour of the model parameters in the standard elliptical accretion disk model applied to describe the broad H α . In each panel, sold circle plus error bars in red mark the positions of the accepted values and the corresponding 1σ uncertainties of the model parameters. The number densities related to different colors are shown in color bar in the left region of each panel.

acceptable, due to seriously obscurations on central continuum emissions. Meanwhile, we measured the stellar velocity dispersion to be 113 ± 10 km/s. Moreover, in order to show the stellar velocity dispersion, the bottom panels of Fig. 1 show the SSP method determined the best descriptions and the corresponding residuals (SDSS spectrum minus the best descriptions and then divided by the uncertainties of SDSS spectrum) to the absorption features around Ca II H+K from 3880 to 4400Å and around Mg I from 5050 to 5300Å.

After subtractions of the host galaxy contributions, more apparent blue-shifted broad H α can be found. And the emission lines can be measured by multiple Gaussian functions, similar as what we have recently done in Zhang (2021a,b, 2022a,b,c). Considering the double-peaked features in the narrow emission lines (especially in the narrow Balmer lines, the [O III] doublet and the [N II] doublet) in SDSS J1052+1036, three Gaussian functions are applied to describe each narrow emission line: two narrow Gaussian components for the double-peaked feature and one Gaussian component for the probably extended emissions underneath the double-peaked feature. Therefore, for the emission lines within the rest wavelength from 4830Å to 5020Å and from 6200Å to 6800Å, there are three Gaussian functions applied to describe the double-peaked narrow H β (H α), one broad Gaussian function to describe the probable broad H β , two

broad Gaussian functions to describe the broad H α , six Gaussian functions to describe the [O III] λ 4959, 5007Å doublet, six Gaussian functions to describe the [N II] λ 6549, 6585Å doublet, one Gaussian function to describe each line in the [O I] λ 6300, 6363Å and the [S II] λ 6716, 6731Å doublets without apparent double-peaked features. When the functions above are applied, each Gaussian component has line intensity not smaller than zero, and the corresponding [O III] ([N II]) components have the same redshift and the same line width and have the flux ratio to be fixed to the theoretical value 3.

Then, through the MPFIT package, the best fitting results (in top regions) and the corresponding residuals (in bottom regions) to the emission lines around H β and H α are shown in the top left panel and the top right panel of Fig. 2 with $\chi^2/dof \sim 0.89$ and $\chi^2/dof \sim 0.88$, respectively. Based on the best fitting results, it is not necessary to consider broad Gaussian component in the H β , because the determined line width and line flux (around to zero) of the broad Gaussian component are smaller than their corresponding uncertainties, indicating not apparent broad H β in SDSS J1052+1036. Moreover, as shown in the top right panel of Fig. 2, each line in the [O I] and [S II] doublets can be well described by one Gaussian component, and whether two or three Gaussian components applied to describe each line in the [O I] and [S II] doublets have few effects on our discussed

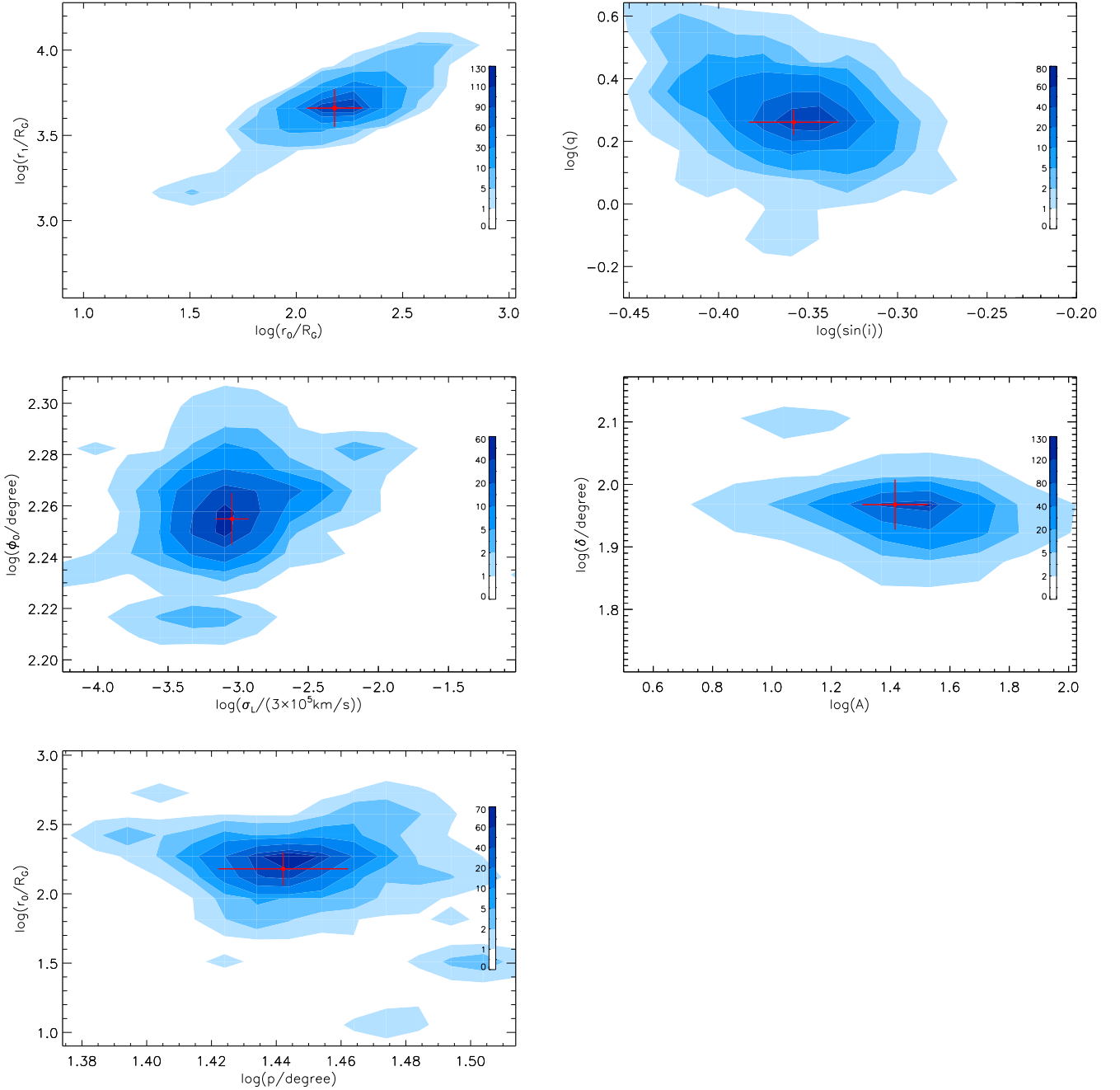


Figure 4. MCMC technique determined two-dimensional posterior distributions in contour of the model parameters in the circular disk plus arm model applied to describe the broad H α . In each panel, solid circle plus error bars in red mark the positions of the accepted values and the corresponding 1σ uncertainties of the model parameters. The number densities related to different colors are shown in color bar in the left region of each panel.

results on the broad H α . The parameters of the Gaussian components applied to describe the emission lines are listed in the Table 1. Based on the best descriptions to the stellar absorption features in Fig. 1 and the best fitting results to the broad H α in the top right panel of Fig. 2, about 2200km/s blue-shifted broad H α can be confirmed.

Besides the broad H α described by two Gaussian components, the blue-shifted broad H α can also be described by the known elliptical accretion disk model discussed in Eracleous et al. (1995), similar as what we have recently done on double-peaked broad

emission lines in Zhang (2021c, 2022a). The elliptical accretion disk model have seven model parameters, inner and out boundaries $[r_0, r_1]$ in unit of R_G (Schwarzschild radius), inclination angle i of disk-like BLRs, eccentricity e , orientation angle ϕ_0 of elliptical rings, local broadening velocity σ_L in units of km/s, line emissivity slope q ($f_r \propto r^{-q}$). In order to obtain more reliable model parameters and corresponding uncertainties, the Maximum Likelihood method combining with the MCMC (Markov Chain Monte Carlo) technique (Foreman-Mackey et al. 2013) is applied. The

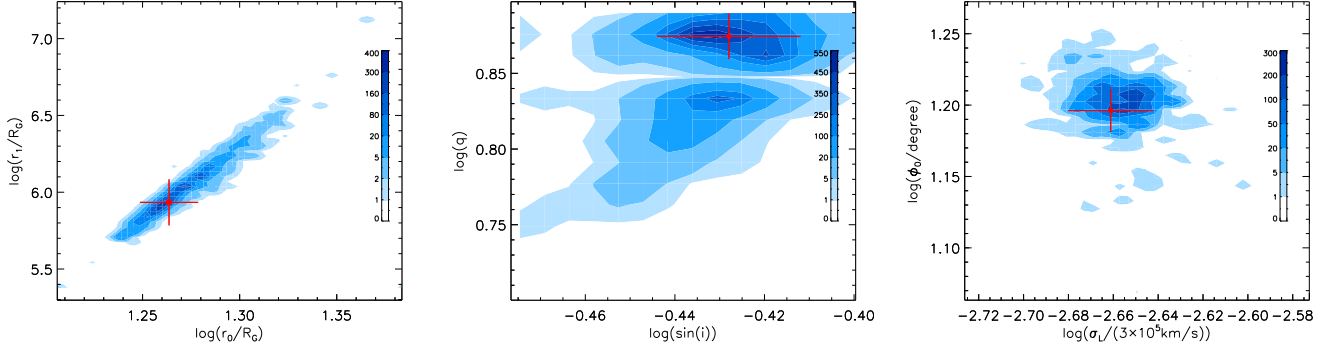


Figure 5. MCMC technique determined two-dimensional posterior distributions in contour of the model parameters in the pure symmetric circular disk model applied to describe the broad H α . In each panel, solid circle plus error bars in red mark the positions of the accepted values and the corresponding 1σ uncertainties of the model parameters. The number densities related to different colors are shown in color bar in the left region of each panel.

evenly prior distributions of the seven model parameters are accepted with the following limitations, $\log(r_0) \in [1, 3]$, $\log(r_1) \in [2, 6]$ ($r_1 > r_0$), $\log(\sin(i)) \in [-3, 0]$, $\log(q) \in [-1, 1]$, $\log(\sigma_L) \in [2, 4]$, $\log(e) \in [-5, 0]$, $\log(\phi_0) \in [-5, \log(2 \times \pi)]$. The determined best fitting results and corresponding residuals to the emission lines around H α are shown in the top region and the bottom region of the middle left panel of Fig. 2 with $\chi^2/dof = 324.41/391 \sim 0.83$. And the model determined best descriptions to the broad H α are shown as solid blue line in the top region of the middle left panel of Fig. 2. The MCMC technique determined posterior distributions of the model parameters in the elliptical accretion disk model are shown in Fig. 3. The determined parameters and the corresponding 1σ uncertainties are listed in the Table 2. Moreover, as discussed in Zhang (2022a), clean double-peaked broad line emission features can lead to solely determined model parameters in the elliptical accretion disk model. Therefore, there are no further discussions on whether is there solely determined model parameters, due to the apparent blue peak in broad H α in SDSS J1052+1036.

Meanwhile, as suggested in Eracleous et al. (2009); Storchi-Bergmann et al. (2003, 2017), rather than the elliptical accretion disk model, the spiral arm rotation is the preferred explanation for most disk emitter profile evolution. Therefore, the circular disk plus spiral arm model with 10 model parameters is also applied to describe the shifted broad H α of SDSS J1052+1036. Besides the model parameters ($e = 0$) applied in the elliptical accretion disk model, four additional model parameters are applied to describe structures of spiral arms, the azimuthal width δ , the pitch angle p and the innermost radius r_m of the spiral arm, and the brightness contrast A between the spiral arm and the underlying axisymmetric disk. Then, based on the new emissivity formula shown in Equation (2) in Storchi-Bergmann et al. (2003) and accepted $r_m = r_0$, the best descriptions and the corresponding residuals to the emission lines around the H α are shown in the middle right panel of Fig. 2 with $\chi^2/dof = 287.88/389 \sim 0.74$. And the model determined best descriptions to the broad H α are shown as solid blue line in the top region of the middle right panel of Fig. 2. The MCMC technique determined posterior distributions of the model parameters in the circular disk plus arm model are shown in Fig. 4. The determined model parameters and the corresponding 1σ uncertainties are also listed in the Table 2 for the circular disk plus arm model.

Table 1. parameters of the emission line components described by Gaussian functions

| line | λ_0 Å | σ Å | flux 10^{-17} erg/s/cm 2 |
|--------------------------------|---------------------|------------------|----------------------------------|
| broad H α | 6511.48 ± 1.06 | 35.12 ± 1.08 | 1036.8 ± 29.2 |
| | 6603.21 ± 11.56 | 22.72 ± 7.09 | 144.6 ± 66.1 |
| Narrow H α | 6558.81 ± 0.31 | 1.32 ± 0.38 | 26.5 ± 11.4 |
| | 6569.66 ± 0.21 | 1.97 ± 0.31 | 89.5 ± 27.3 |
| | 6564.69 ± 0.43 | 5.21 ± 0.18 | 626.3 ± 42.2 |
| Narrow H β | 4858.38 ± 0.68 | 1.18 ± 0.83 | 7.8 ± 8.4 |
| | 4866.56 ± 0.28 | 1.42 ± 0.34 | 24.9 ± 9.9 |
| | 4862.18 ± 0.38 | 3.37 ± 0.75 | 72.1 ± 19.7 |
| [O III] $\lambda 5007\text{Å}$ | 5005.81 ± 0.25 | 2.38 ± 0.31 | 327.6 ± 141.4 |
| | 5011.71 ± 0.11 | 2.13 ± 0.11 | 515.9 ± 74.2 |
| | 5007.72 ± 0.41 | 5.09 ± 0.82 | 383.2 ± 200.2 |
| [O I] $\lambda 6300\text{Å}$ | 6302.43 ± 0.44 | 4.86 ± 0.46 | 72.1 ± 6.1 |
| [O I] $\lambda 6363\text{Å}$ | 6364.26 ± 0.87 | 4.05 ± 0.89 | 26.3 ± 5.1 |
| [N II] $\lambda 6583\text{Å}$ | 6580.86 ± 1.27 | 3.18 ± 0.73 | 90.1 ± 68.1 |
| | 6589.87 ± 0.38 | 1.93 ± 0.52 | 53.8 ± 32.3 |
| | 6585.35 ± 0.44 | 5.22 ± 0.18 | 422.1 ± 105.3 |
| [S II] $\lambda 6716\text{Å}$ | 6720.47 ± 0.57 | 6.51 ± 0.49 | 232.6 ± 17.7 |
| [S II] $\lambda 6731\text{Å}$ | 6734.97 ± 0.58 | 4.34 ± 0.45 | 108.6 ± 15.6 |

Notice: For the Gaussian components, the first column shows which line is measured, the second, third, fourth columns show the measured line parameters: center wavelength λ_0 in unit of Å, line width (second moment) σ in unit of Å and line flux in unit of 10^{-17} erg/s/cm 2 .

3 MAIN DISCUSSIONS

3.1 A kpc-scale dual core system in SDSS J1052+1036?

Double-peaked [O III] $\lambda 5007\text{Å}$ can be seen in the spectrum of SDSS J1052+1036, as well as shown in Ge et al. (2012), widely indicating a kpc-scale dual core system (Zhou et al. 2004; Xu & Komossa 2009; Fu et al. 2011; Wang et al. 2019). Based on the measured double-peaked features in the [O III] $\lambda 5007\text{Å}$, the peak separation is about 350 ± 22 km/s in SDSS J1052+1036, leading the broad emission lines from the assumed central two cores to have the same peak separa-

Table 2. model parameters of accretion disk models for the broad H α

| |
|---|
| the elliptical accretion disk model $r_0 = 38 \pm 2$, $r_1 = 490 \pm 35$, $\sin(i) = 0.48 \pm 0.04$ $q = 0.17 \pm 0.01$, $e = 0.56 \pm 0.03$, $\sigma_L = 850 \pm 40$ km/s $\phi_0 = 237 \pm 5^\circ$ |
| the circular disk plus spiral arm model $r_0 = 150 \pm 60$, $r_1 = 4500 \pm 1300$, $\sin(i) = 0.44 \pm 0.04$, $q = 1.82 \pm 0.21$ $\sigma_L = 270 \pm 90$ km/s, $\phi_0 = 179 \pm 3^\circ$, $A = 26 \pm 7$ $\delta = 93 \pm 10^\circ$, $p = 28 \pm 2^\circ$ |
| the pure symmetric circular disk model $r_0 = 18 \pm 1$, $r_1 = (8 \pm 3) \times 10^5$, $\sin(i) = 0.37 \pm 0.01$, $q = 7.48 \pm 0.91$ $\sigma_L = 650 \pm 103$ km/s, $\phi_0 = 16 \pm 3^\circ$ |
| the elliptical accretion disk model with $V_s = -265$ km/s $r_0 = 31 \pm 2$, $r_1 = 246 \pm 25$, $\sin(i) = 0.33 \pm 0.03$ $q = 0.66 \pm 0.05$, $e = 0.58 \pm 0.03$, $\sigma_L = 916 \pm 60$ km/s $\phi_0 = 240 \pm 6^\circ$ |
| the elliptical accretion disk model with $V_s = 231$ km/s $r_0 = 44 \pm 4$, $r_1 = 381 \pm 40$, $\sin(i) = 0.38 \pm 0.04$ $q = 1.26 \pm 0.15$, $e = 0.54 \pm 0.03$, $\sigma_L = 532 \pm 30$ km/s $\phi_0 = 240 \pm 6^\circ$ |

tion 350km/s. However, the peak separation about 4200 ± 580 km/s between the blue-shifted broad component and the red-shifted broad component in the broad H α in SDSS J1052+1036 is about twelve times higher than the peak separation of the double-peaked narrow emission lines. Therefore, the shifted broad H α is not related to a kpc-scale dual core system expected by the double-peaked [O III] in SDSS J1052+1036.

3.2 A rSMBH in SDSS J1052+1036?

One another explanation for the blue shifted broad H α in SDSS J1052+1036 is that it is a rSMBH, after considering materials in the BLRs being carried away with the rSMBH. Meanwhile, not a single but two broad Gaussian components in the broad H α in SDSS J1052+1036 are probably indicating asymmetric structures of the BLRs bound to the rSMBH. As discussed in Merritt et al. (2006); Gualandris & Merritt (2008); Komossa & Merritt (2008b), the materials in the BLRs can be bound to a rSMBH within a region with the radius r_k given by

$$r_k \sim 512 \frac{M_{BH}}{10^8 M_\odot} \left(\frac{V_k}{10^3 \text{km/s}} \right)^{-2} \text{light - days} \quad (1)$$

with M_{BH} and V_k as the BH mass and the kick velocity of a rSMBH. Meanwhile, in order to support a rSMBH by blue-shifted broad emission lines, the blue-shifted broad emission component related to the emission materials bound to a rSMBH should be apparent enough, indicating almost all the materials in the original BLRs bound to the rSMBH. Therefore, we can expect that the estimated r_k should be not smaller than the origin BLRs size R_{BLRs} which can be estimated by the continuum luminosity $L_{5100\text{\AA}}$ at 5100 \AA (Bentz et al. 2013),

$$\frac{r_k}{\text{light - days}} \geq \frac{R_{BLRs}}{\text{light - days}} = 10^{1.555+0.542 \times \log\left(\frac{L_{5100\text{\AA}}}{10^{44} \text{erg/s}}\right)} \quad (2)$$

In SDSS J1052+1036 with the well measured stellar velocity dispersion about 113 ± 10 km/s, after considering the M-sigma relation discussed in Ferrarese & Merritt (2000); Gebhardt et al. (2000); Kormendy & Ho (2013); Batiste et al. (2017); Bennert et al. (2021)

for both quiescent and active galaxies and also as discussed in Di Matteo et al. (2005); Johansson et al. (2009) in galaxy merging systems, the BH mass can be estimated as $2.5^{+2.2}_{-1.3} \times 10^7 M_\odot$ in SDSS J1052+1036, accepted Equation (7) in Kormendy & Ho (2013). Therefore, based on the equation above, we could have $L_{5100} < 4 \times 10^{43}$ erg/s, which can lead to apparent blue-shifted broad H α totally related to an expected rSMBH.

Based on the determined continuum emissions in the top panel of Fig. 1, the observed continuum luminosity at 5100 \AA is about 6.3×10^{42} erg/s in SDSS J1052+1036. Accepted the intrinsic L_{5100} should be smaller than 4×10^{43} erg/s, the intrinsic obscuration should have $E(B-V) \leq 0.6$. Then, accepted the intrinsic flux ratio 3.1 of broad H α to broad H β , the expected observed flux ratio of the broad H α to the broad H β should be smaller than 6.2, leading to a detectable blue-shifted broad component in the H β in SDSS J1052+1036. Unfortunately, as shown in the top left panel of Fig. 2, there are no detectable broad components in the H β in SDSS J1052+1036. Therefore, the blue-shifted broad H α probably contains weak contributions from a rSMBH scenario in SDSS J1052+1036.

Unfortunately, the discussions above are not sufficient enough to totally disfavour the rSMBH scenario in SDSS J1052+1036, however, multi-epoch spectroscopic results should provide clear clues to support or to be against the rSMBH scenario. If the expected rSMBH in SDSS J1052+1036 moves rectilinearly (or moves curvilinearly as the case in Mrk 1018 in Kim et al. 2018), very tiny (or no) changes of peak separations between the blue-shifted component and the red-shifted component in the broad H α could be expected in SDSS J1052+1036.

3.3 A BBH system in SDSS J1052+1036?

If a BBH system was accepted in SDSS J1052+1036 with the estimated total BH mass $2.5^{+2.2}_{-1.3} \times 10^7 M_\odot$ by the $M_{BH} - \sigma$ relation, the two broad Gaussian components in the broad H α could be simply accepted to estimate the observational peak separation about $V_{p,obs} = 4200 \pm 600$ km/s, leading the upper limit of the space separation S of the central two BHs to be

$$S < \frac{G \times M_{BH}}{V_{p,obs}^2} \sim 7.3^{+11.3}_{-4.6} \text{light - days} \quad (3)$$

Based on the measured luminosity 2.01×10^{41} erg/s of the observed broad H α or the measured continuum luminosity 6.2×10^{42} erg/s at 5100 \AA in the rest frame, the estimated BLRs size should be about 7light-days, after considering the correlation between broad H α luminosity and continuum luminosity discussed in Greene & Ho (2005) and the empirical R-L relation discussed in Bentz et al. (2013).

However, considering SDSS J1052+1036 as a Type-1.9 AGN, serious obscuration indicates the intrinsic BLRs size should be much larger than 7light-days. The BLRs size is similar as the upper limit of space separation of the central two BHs, strongly indicating the two BLRs probably totally mixed, leading to no apparent variability in the peak positions in the broad H α , as discussed in Shen & Loeb (2010). Moreover, under the assumption of a BBH system in SDSS J1052+1036, probable optical quasi-periodic oscillations (Graham et al. 2015a,b; Zheng et al. 2016; Zhang 2022d,e, 2023) should be detected. However, after checking long-term light curves from Catalina Sky Survey (Drake et al. 2009), All-Sky Automated Survey for Supernovae (Shappee et al. 2014; Kochanek et al. 2017) and Zwicky Transient Facility (Bellm et al. 2019; Dekany et al. 2020), there is no significant variability, which can not provide clues to support a BBH system in SDSS J1052+1036.

Meanwhile, under the assumption of a BBH system in SDSS J1052+1036, considering the stronger and wider broad blue-shifted component in the $H\alpha$ ($H\alpha_B$), the virial BH mass $M_{BH,B}$ related to the $H\alpha_B$ should be simply expected to be 6.4 times larger than the virial BH mass $M_{BH,R}$ related to the red-shifted broad component in the $H\alpha$ ($H\alpha_R$), accepted the virialization assumptions to the broad emission lines as discussed in [Greene & Ho \(2005\)](#); [Peterson et al. \(2004\)](#). Here, the factor 6.4 is simply calculated by $(\frac{1036.8}{144.6})^{0.5} (\frac{35.12}{22.72})^2$ with 1036.8 and 144.6 (35.12 and 22.72) as the line fluxes (the line widths) of the $H\alpha_B$ and the $H\alpha_R$ in SDSS J1052+1036. Then, the $H\alpha_B$ should have 6.3 times smaller shifted velocity than that of the $H\alpha_R$, which is against the measured results that the shifted velocity $2430\pm 50\text{km/s}$ of the $H\alpha_B$ is larger than the shifted velocity about $1760\pm 530\text{km/s}$ of the $H\alpha_R$, indicating a BBH system is disfavoured in SDSS J1052+1036.

Furthermore, if we accepted the double-peaked narrow emission lines as signs of kpc-scale dual core systems and also accepted the blue-shifted broad $H\alpha$ related to a BBH system, there should be a rare close-pair binary in a triple BH system in SDSS J1052+1036, similar as those discussed in [Hoffman & Loeb \(2007\)](#); [Deane et al. \(2014\)](#). In such a rare close-pair binary in a triple BH system in SDSS J1052+1036, similar results can be expected that the shifted velocity of the $H\alpha_B$ should be quite smaller than that of the $H\alpha_R$. However, whether the red-shifted (or the blue-shifted) narrow emission component in the double-peaked narrow $H\alpha$ is applied to trace the rotating velocity of the close-pair binary BH system in a triple BH system, larger shifted velocity of the $H\alpha_B$ can be determined than that of the $H\alpha_R$. Therefore, a close-pair binary in a triple BH system is disfavoured in SDSS J1052+1036

3.4 A disk emitter in SDSS J1052+1036?

Based on the model parameters of the elliptical accretion disk model listed in the Table 2, the expected disk precession period should be about $T_{\text{pre}} \sim 1040M_8R_3^{2.5}\text{yr}$. Using the $M_{BH} - \sigma$ determined BH mass $M_8 \sim 0.25^{+0.22}_{-0.13}$ in units of 10^8M_\odot and R_3 as radius in units of $1000R_G$, based on the determined r_0 , r_1 and q , the flux weighted size of the emission regions for the broad $H\alpha$ to the central BH is about $248R_G$, leading to an approximately estimated disk precession period of 8years. As well known, asymmetric structures in accretion disk model are key factors leading to apparent variabilities of the peak positions and the peak separations of the double-peaked broad emission lines due to pure disk precessions, which will provide clues to support a disk emitter in SDSS J1052+1036. If there should be a re-observed spectrum in Jul. 2025 (MJD~60858), based on the expected precession period of about 8years, the expected line profiles of the broad $H\alpha$ in SDSS J1052+1036 in 2025 are shown as dotted blue line and dot-dashed blue line in the top region of the middle left panel of Fig. 2 with considering the standard elliptical accretion disk model applied with anti-clockwise rotation and clockwise precessions respectively.

Meanwhile, it is necessary to check whether a pure symmetric circular accretion disk model (with eccentricity to be zero) (without spiral arms) can be applied to describe the observed shifted broad $H\alpha$ in SDSS J1052+1036. For a circular accretion disk model with $e = 0$, a similar fitting procedure is applied to describe the broad $H\alpha$ in SDSS J1052+1036, with the final determined fitting results to the broad $H\alpha$ shown as dashed blue line in the top region of the middle left panel of Fig. 2 with corresponding $\chi^2/dof = 469.37/392 \sim 1.21$. The MCMC technique determined posterior distributions of the model parameters in the pure symmetric circular disk model are shown in

Fig. 5. The determined model parameters and the corresponding 1σ uncertainties are also listed in the Table 2 for the pure symmetric circular disk model. Based on the F-test technique similar as what we have recently done in [Zhang \(2022c\)](#), due to the different values of χ^2 and dof for the different accretion disk models, the confidence level can be determined to be higher than 6σ to support that the elliptical accretion disk model and the circular accretion disk plus arm model is preferred than the pure symmetric circular accretion disk model. Unfortunately, only through the single-epoch spectroscopic properties of SDSS J1052+1036, we can not find more clues to support that the pure symmetric circular disk model is totally disfavored in SDSS J1052+1036. Therefore, in the manuscript, the pure symmetric circular disk model is also accepted as a reasonable model to describe the shifted broad $H\alpha$ in SDSS J1052+1036.

Moreover, if accepted the double-peaked features in the $[\text{O III}]\lambda 4959, 5007\text{\AA}$ doublet as signs of a kpc-scale dual core system, a rotating disk emitter (disk emission regions with a rotating velocity related to the orbital motions of central dual cores) contained in a dual core system could also be applied to describe the observed blue-shifted broad $H\alpha$ in SDSS J1052+1036. Considering the double-peaked features in the narrow $H\alpha$ to trace the rotating velocity V_s of the disk emitter in a dual core system, the best fitting results and the corresponding residuals to the emission lines around $H\alpha$ can be re-determined with $V_s = -265\text{km/s}$ and with $V_s = 231\text{km/s}$, and shown in the bottom left panel and the bottom right panel of Fig. 2 with corresponding $\chi^2/dof \sim 1.03$ and $\chi^2/dof \sim 1.02$, respectively. The model determined broad $H\alpha$ after considering V_s are shown as solid blue lines in the top regions of the bottom panels of Fig. 2. Moreover, if considering the elliptical accretion disk model with V_s in SDSS J1052+1036, there are similar 1σ uncertainties of the model parameters as those of the standard elliptical accretion disk model shown in Fig. 3. Therefore, we did not show the posterior distributions of the model parameters for the rotating elliptical disk models, but the model parameters and the corresponding 1σ uncertainties are listed in the Table 2. Based on the determined model parameters listed in the Table 2 for the rotating elliptical accretion disk model with V_s , disk precession periods can be estimated as 1.68years and 4.95years, with the central wavelengths of the blue-shifted component and the red-shifted component in the narrow $H\alpha$ applied to determine the V_s . Then, the expected line profiles of the broad $H\alpha$ in SDSS J1052+1036 in Jul. 2025 are shown as dotted blue line and dot-dashed blue line in the top regions of the bottom left panel and the bottom right panel of Fig. 2 with considering the elliptical accretion disk model with $V_s = -265\text{km/s}$ and $V_s = 231\text{km/s}$ applied with anti-clockwise rotation and clockwise precessions respectively.

Either a rotating elliptical disk emitter contained in a dual core system or a standard elliptical disk emitter can lead to apparent time dependent variations of the peak positions and the peak separations of the shifted broad $H\alpha$ in SDSS J1052+1036 as a disk emitter. Considering different disk precession periods determined by standard accretion disk model and/or rotating disk emitter, if there should be a re-observed spectrum in Jul. 2025, the expected broad $H\alpha$ in 2025 in SDSS J1052+1036 have quite different peak positions and different peak separations from the broad $H\alpha$ in the SDSS spectrum observed in MJD=53117. Therefore, a re-observed spectrum in 2025 should provide clues enough to confirm whether a disk emitter is preferred in SDSS J1052+1036. Unfortunately, unless there are detailed time-dependent variabilities of the broad $H\alpha$ in SDSS J1052+1036, it is hard to distinguish a standard elliptical disk emitter from a rotating elliptical disk emitter in a kpc-scale dual core system.

Furthermore, if considering the circular disk plus spiral arm model

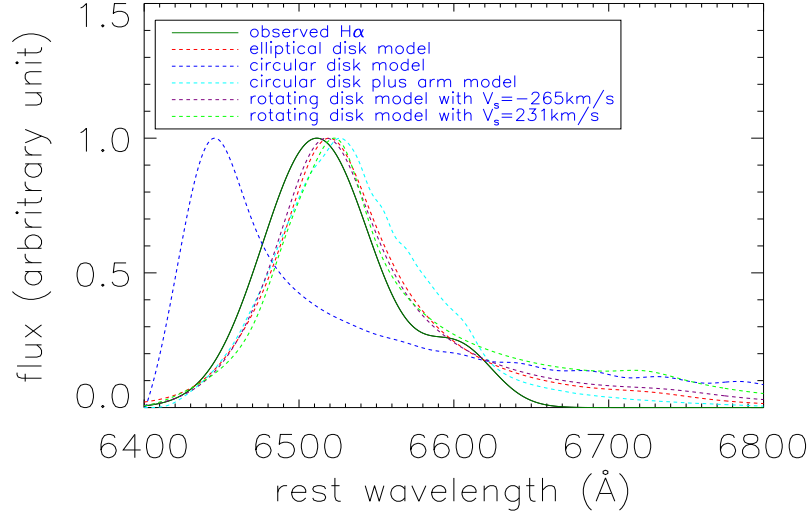


Figure 6. Expected line profiles of the shifted broad H α with only r_0 and r_1 changed in the different accretion disk models. As described in the legend, besides the solid dark green line representing the observed shifted broad H α described by two broad Gaussian functions, each other dashed line in different color represents the corresponding model expected line profile of the shifted broad H α in different epoch with only r_0 and r_1 changed.

in SDSS J1052+1036, the expected disk precession period should be about 2100 years, due to the quite large flux weighted size $R_3 \sim 2.3$ of the emission regions of the blue-shifted broad H α to the central BH. Meanwhile, the precessing spiral pattern could have precession period more than 100 years, considering ten times of the dynamical time of accretion disk as discussed in Storchi-Bergmann et al. (2003). The large precession periods strongly indicate no apparent variabilities of profiles of the broad H α in SDSS J1052+1036, if considering the circular disk plus arm model to describe the shifted broad H α . However, as discussed in Storchi-Bergmann et al. (2003), the model parameters of A , q are varying in the circular disk plus spiral arm model. The varying parameter of A can lead to apparent variability of the peak intensity ratio of the broad H α of SDSS J1052+1036. As an example, if A was changed from 26 to 5 in 2025, quite stronger red peak could be possibly expected in the broad H α of SDSS J1052+1036, as shown in the top region of the middle right panel of Fig. 2. Similar results can be found, if the circular plus arm model discussed in a dual core system. Therefore, there are no plots or discussions for the corresponding results based on the circular plus arm contained in a dual core system.

Before the end of the subsection, an additional point should be noted. Discussions above on variations of the profiles of the shifted broad H α are due to pure disk precessions in SDSS J1052+1036 as a disk emitter, which can lead to apparent variations from the elliptical accretion disk model but no apparent variations from the circular disk model neither from the circular plus arm model. However, effects of variability of AGN activities should also have apparent effects on the variations of profiles of the shifted broad H α in SDSS J1052+1036 as a disk emitter, which will be discussed as follows.

Sizes R_{BLR_s} of central BLRs of dozens of broad line AGN have been measured through the reverberation mapping technique (Blandford & McKee 1982; Peterson 1993; Peterson et al. 1999; Barth et al. 2015; Du et al. 2018; Shen et al. 2019b; Lu et al. 2023), leading to the known dependence of R_{BLR_s} on AGN continuum luminosity (or on broad line luminosity) (Kaspi et al. 2000; Bentz et al. 2013). Therefore, stronger central AGN emissions can lead to deeper

ionization boundaries of central BLRs, in other words, stronger AGN emissions can lead to larger R_{BLR_s} . Therefore, if there was apparent variability of AGN activities in SDSS J1052+1036, different inner radius and outer radius in different epochs could be expected from those listed in the Table 2 of the different accretion disk models for shifted broad H α shown in Fig. 2, leading to probably different line profiles. As an example, if we assumed that there was a spectrum observed again at any time but with the re-observed AGN continuum luminosity at 5100 Å about 2 times of the AGN continuum luminosity shown in the top panel of Fig. 1, leading the expected R_{BLR_s} to be 1.4 times larger than the R_{BLR_s} for the shifted broad H α shown in Fig. 2. Then, the re-determined inner radius and outer radius of the different disk models should be approximately 1.4 times of the r_0 and r_1 listed in the Table 2. Based on the re-determined inner radius and outer radius and the other model parameters which remain unchanged, the model expected line profiles are shown in Fig. 6 only considering AGN variability, leading to apparent variations of the line profiles of the shifted broad H α by different accretion disk models (even the pure symmetric circular disk model) in different epochs, strongly different from the expected results by the rSMBH scenario. Therefore, besides the accretion disk precessions, strong AGN variations have also apparent effects on variations of the profiles of the shifted broad H α , which will provide further clues to support SDSS J1052+1036 as a disk emitter.

4 MAIN SUMMARY AND CONCLUSIONS

A rare low-redshift Type-1.9 AGN SDSS J1052+1036 but with very blue-shifted broad H α is reported in this manuscript. The main summary and conclusions are as follows.

- The very blue-shifted broad H α is not related to a kpc-scale dual core system in SDSS J1052+1036 with apparent double-peaked narrow emission lines, due to quite different peak separations of the double-peaked narrow emission lines from the peak separation of the

blue-shifted component and the red-shifted component in the broad $H\alpha$.

- The very blue-shifted broad $H\alpha$ is not related to a sub-pc BBH system in SDSS J1052+1036, due to stronger and wider blue-shifted $H\alpha$ having larger shifted velocity.

- The very blue-shifted broad $H\alpha$ probably does not arise due to the rSMBH scenario, mainly due to rSMBH scenario expected obscuration having $E(B-V) \leq 0.6$, leading to probably detectable broad components in the $H\beta$, against the spectroscopic results without broad $H\beta$ in SDSS J1052+1036.

- The very blue-shifted broad $H\alpha$ can be well explained by a disk emitter in SDSS J1052+1036 without any caveats.

- Due to disk precessions of accretion disk models, the standard elliptical accretion disk model can lead to apparent variations of the profiles of the shifted broad $H\alpha$ in SDSS J1052+1036 as a disk emitter, however no apparent variations could be expected in recent years through the circular disk model or the circular plus arm model.

- If considering strong variations of AGN activities leading to variations of ionization boundaries, apparent variations in different epochs can be expected in the profiles of the shifted broad $H\alpha$ in SDSS J1052+1036 as a disk emitter.

- A re-observed spectrum in 2025 could provide robust clues to support a disk emitter in SDSS J1052+1036, if there were apparent variations of peak positions, peak separations and/or peak intensity ratios in the broad $H\alpha$.

ACKNOWLEDGEMENTS

Zhang gratefully acknowledges the anonymous referee for giving us constructive comments and suggestions to greatly improve our paper. Zhang gratefully acknowledges the kind financial support from GuangXi University and the kind funding support NSFC-12173020 and NSFC-12373014. This research has made use of the data from the SDSS (<https://www.sdss.org/>) funded by the Alfred P. Sloan Foundation, the Participating Institutions, the National Science Foundation and the U.S. Department of Energy Office of Science. The research has made use of the MPFIT package <https://pages.physics.wisc.edu/~craigm/idl/cmpfit.html>, and of the emcee package <https://pypi.org/project/emcee/>.

DATA AVAILABILITY

The data underlying this article will be shared on request to the corresponding author (xgzhang@gxu.edu.cn).

REFERENCES

Barth, A. J.; Bennert, V. N.; Canalizo, G.; Filippenko, A. V.; Gates, E. L., 2015, *ApJS*, 217, 26
 Batiste, M.; Bentz, M. C.; Raimundo, S. I.; Vestergaard, M.; Onken, C. A., 2017, *ApJL*, 838, 10
 Bekenstein, J. D. 1973, *ApJ*, 183, 657
 Bellm E. C., Kulkarni, S. R.; Barlow, T., et al., 2019, *PASP*, 131, 068003
 Blandford, R. D.; McKee, C. F., 1982, *ApJ*, 255, 419
 Blecha, L., Loeb, A. 2008, *MNRAS*, 390, 1311
 Blecha, L., Sijacki, D., Kelley, L. Z., et al. 2016, *MNRAS*, 456, 961
 Bennert, V. N.; Treu, T.; Ding, X.; et al., 2021, *ApJ*, 921, 36
 Bentz, M. C.; Denney, K. D.; Grier, C. J., et al., 2013, *ApJ*, 767, 149
 Bogdanovic, T.; Eracleous, M.; Sigurdsson, S., 2009, *ApJ*, 697, 288
 Bruzual, G.; Charlot, S. 2003, *MNRAS*, 344, 1000
 Cappellari, M., 2017, *MNRAS*, 466, 798

Chiaberge, M.; Ely, J. C.; Meyer, E. T.; et al., 2017, *A&A*, 600, 57
 Chiaberge, M.; Tremblay, G. R.; Capetti, A.; Norman, C., 2018, *ApJ*, 861, 56
 Cid Fernandes, R.; Mateus, A.; Sodre, L.; Stasinska, G.; Gomes, J. M., 2005, *MNRAS*, 358, 363
 Deane, R. P.; Paragi, Z.; Jarvis, M. J.; et al., 2014, *Natur*, 511, 57
 Dekany, R.; Smith, R. M.; Riddle, R., et al., 2020, *PASP*, 132, 038001
 Di Matteo, T.; Springel, V.; Hernquist, L., *Natur*, 433, 604
 Drake, A. J.; Djorgovski, S. G.; Mahabal, A.; et al., 2009, *ApJ*, 696, 870
 Du, P.; Zhang, Z.-X.; Wang, K.; Huang, Y.-K.; Zhang, Y.; et al., 2018, *ApJ*, 856, 6
 Eracleous, M., Livio, M., Halpern, J. P., Storchi-Bergmann, T., 1995, *ApJ*, 438, 610
 Eracleous, M.; Lewis, K. T.; Flohic, H. M. L. G., *NewAR*, 53, 133
 Eracleous, M.; Boroson, T. A.; Halpern, J. P.; Liu, J., 2012, *ApJS*, 201, 23
 Ferrarese, F.; Merritt, D., 2000, *ApJL*, 539, 9
 Foreman-Mackey, D.; Hogg, D. W.; Lang, D.; Goodman, J., 2013, *PASP*, 125, 306
 Fu, H.; Zhang, Z.; Assef, R. J., et al., 2011, *ApJL*, 740, 44
 Ge, J.; Hu, C.; Wang, J.; Bai, J.; Zhang, S., 2012, *ApJS*, 201, 31
 Gebhardt, K.; Bender, R.; Bower, G., et al., 2000, *ApJL*, 539, 13
 Graham, M. J.; Djorgovski, S. G.; Stern, D., et al., 2015a, *Natur*, 518, 74
 Graham, M. J.; Djorgovski, S. G.; Stern, D., et al., 2015b, *MNRAS*, 453, 1562
 Greene, J. E.; Ho, L. C., 2005, *ApJ*, 630, 122
 Gualandris, A.; Merritt, D., 2008, *ApJ*, 678, 180
 Hoffman, L.; Loeb, A., 2007, *MNRAS*, 377, 957
 Johansson, P.; Naab, T.; Burkert, A., 2009, *ApJ*, 690, 802
 Kalfountzou, E.; Santos Lleo, M.; Trichas M., 2017, *ApJL*, 851, 15
 Kaspi, S.; Smith, P. S.; Netzer, H.; Maoz, D.; Jannuzi, B. T.; Giveon, U., 2000, *ApJ*, 533, 631
 Kauffmann, G.; Heckman, T. M.; Tremonti, C., et al. 2003, *MNRAS*, 346, 1055
 Kim, D. C.; Evans, A. S.; Stierwalt, S.; Privon, G. C., 2016, *ApJ*, 824, 122
 Kim, D. C.; Yoon, I.; Privon, G. C.; Evans, A. S.; Harvey, D.; Stierwalt, S.; Kim, J. H., 2017, *ApJ*, 840, 71
 Kim, D. C.; Yoon, I.; Evans, A. S., 2018, *ApJ*, 861, 51
 Kochanek, C. S.; Shappee, B. J.; Stanek, K. Z.; et al., 2017, *PASP*, 129, 4502
 Komossa, S., Merritt, D., 2008a, *ApJL*, 683, 21
 Komossa, S., Merritt, D., 2008b, *ApJL*, 689, 89
 Komossa, S.; Zhou, H.; Lu, H., 2008, *ApJL*, 678, 81
 Kormendy, J.; Ho, L. C., 2013, *ARA&A*, 51, 511
 Lena, D.; Robinson, A.; Marconi, A.; Axon, D. J.; Capetti, A.; Merritt, D.; Batcheldor, D., 2014, *ApJ*, 795, 146
 Lu, K.-X.; Bai, J.-M.; Wang, J.-M.; Hu, C.; Li, Y.-R., 2023, *ApJS*, 263, 10
 Madau, P., Quataert, E. 2004, *ApJL*, 606, 17
 Merritt, D.; Storchi-Bergmann, T.; Robinson, A.; Batcheldor, D.; Axon, D.; Cid Fernandes, R., 2006, *MNRAS*, 367, 1746
 Morishita, T.; Chiaberge, M.; Hilbert, B.; et al., 2022, *ApJ*, 931, 165
 Peterson, B. M., 1993, *PASP*, 105, 247
 Peterson, B. M.; Barth, A. J.; Berlind, P.; Bertram, R.; Bischoff, K.; et al., 1999, *ApJ*, 510, 659
 Peterson, B. M.; Ferrarese, L.; Gilbert, K. M., et al., 2004, *ApJ*, 613, 682
 Popovic, L. C.; Shapovalova, A. I.; Ilic, D., et al., 2014, *A&A*, 572, 66
 Runnoe, J. C.; Eracleous, M.; Mathes, G.; et al., 2015, *ApJS*, 221, 7
 Runnoe, J. C.; Eracleous, M.; Pennell, A.; et al., 2017, *MNRAS*, 468, 1683
 Shappee, B. J.; Prieto, J. L.; Grupe, D.; et al., 2014, *ApJ*, 788, 48
 Shen, Y.; Loeb, A., 2010, *ApJ*, 725, 249
 Shen, Y.; Hwang, H.; Zakamska, N.; Liu, X., 2019, *ApJL*, 885, 4
 Shen, Y.; Hall, P. B.; Horne, K.; Zhu, G.; McGreer, I.; et al., 2019b, *ApJS*, 241, 34
 Shields, G. A.; Rosario, D. J.; Smith, K. L.; et al., 2009, *ApJ*, 707, 936
 Steinhardt, C. L.; Schramm, M.; Silverman, J. D.; et al., 2012, *ApJ*, 759, 24
 Storchi-Bergmann, T.; Nemmen da Silva, R., Eracleous, M., et al., 2003, *ApJ*, 598, 956
 Storchi-Bergmann, T.; Schimoia, J. S.; Peterson, B. M.; Elvis, M.; Denney, K. D.; Eracleous, M.; Nemmen, R. S., 2017, *ApJ*, 835, 236
 Volonteri, M., 2007, *ApJL*, 663, 5
 Wang, M.; Luo, A.; Song, Y., et al., 2019, *MNRAS*, 482, 1889
 Ward, C.; Gezari, S.; Frederick, S.; et al., 2021, *ApJ*, 913, 102

- Xu, D.; Komossa, S., 2009, *ApJL*, 705, 20
Zhang, X. G., 2021d, *MNRAS*, 502, 2508
Zhang, X. G., 2021a, *ApJ*, 909, 16, ArXiv:2101.02465
Zhang, X. G., 2021b, *ApJ*, 919, 13, ArXiv:2107.09214
Zhang, X. G., 2021c, *MNRAS Letter*, 500, 57
Zhang, X. G., 2022a, *ApJS*, 260, 31
Zhang, X. G., 2022b, *ApJS*, 261, 23
Zhang, X. G., 2022c, *ApJ*, 937, 105, ArXiv:2209.02164
Zhang, X. G., 2022d, *MNRAS*, 512, 1003, arXiv:2202.11995
Zhang, X. G., 2022e, *MNRAS*, 516, 3650, arXiv:2209.01923
Zhang, X. G., 2023, *MNRAS* accepted, arXiv:2309.08078
Zheng, Z.; Butler, N. R.; Shen, Y.; et al., 2016, *ApJ*, 827, 56
Zhou, H., Wang, T., Zhang, X., Dong, X., Li, C. 2004, *ApJL*, 604, L33